


Excitonic nonlinear optical properties in AlN/GaN spherical core/shell quantum dots under pressure

N. Aghoutane, M. El-Yadri, A. El Aouami, and E. Feddi, Laboratoire de Matière Condensée et Sciences Interdisciplinaires (LaMCScI), Group of Optoelectronic of Semiconductors and Nanomaterials, ENSET, Mohammed V University in Rabat, Rabat 10100, Morocco

G. Long , and **M. Sadoqi**, Department of Physics, Saint John's University, Jamaica, NY, 11439, USA

F. Dujardin, LCP-A2MC, Université de Lorraine, 57000 Metz, France

Chuong V. Nguyen, Department of Materials Science and Engineering, Le Quy Don Technical University, Hanoi, 100000, Vietnam

Nguyen N. Hieu, Institute of Research and Development, Duy Tan University, Da Nang, 550000, Vietnam

Huynh V. Phuc, Division of Theoretical Physics, Dong Thap University, Cao Lanh, 870000, Vietnam

Address all correspondence to E. Feddi at e.feddi@um5s.net.ma; G. Long at longg@stjohns.edu

(Received 23 January 2019; accepted 26 March 2019)

Abstract

This work is based on a recent theoretical study of how the hydrostatic pressure and core/shell sizes affect the optical properties associated with the transition from the ground state to first excited state ($1s-1p$), of an exciton confined in spherical core/shell quantum dots (SCSQDs). We have computed under an effective mass framework, linear, third-order nonlinear, and total absorption coefficients (AC) and refractive index (RI) as functions of photon energy for different sizes of SCSQDs with varying hydrostatic pressure. Our results show that the optical absorption is deeply dependent on the incident light intensity. Both AC and RI significantly influenced by the confinement and pressure effects.

Introduction

In recent years, thanks to advance in nanomaterial growth and characterization, spherical core/shell quantum dots (SCSQDs) have been widely realized on various material systems and extensively studied experimentally and theoretically.^[1–5] These nanostructures usually consist of an inorganic material (core), which is covered by a layer of another material (shell) with a band gap lower than that of the core (i.e., reverse type-I). The nanostructures can be coated with another material (usually organic molecules as ligands) which stabilizes these nanostructures via the passivation of their surfaces thus prevent their physical degradation and ensure their optical properties. The novel properties of these nanoscale structures arise from quantum confinement effects, and therefore they draw great interest in nanomaterial research community due to their potentially wide variety of applications such as photovoltaics,^[6,7] light-emitting diodes,^[8–10] and nonlinear optics.^[11] Many studies have been realized for SCSQDs.^[12–18] From these results we can conclude that these nanostructures acquire interesting physical properties, such as the enhanced binding energy due to strong confinement when the hydrostatic pressure and magnetic field are applied, plus increased band-edge absorption for small band gap shell materials, as well as the enhanced intensity of luminescence.

Numerous investigations have been carried out on optical properties of these nanostructures, with or without external factors such as applied pressure, temperature, magnetic field,

etc.^[19–22] We have recently studied the linear and nonlinear optical properties of a confined exciton inside an SQD (GaAs) and found that optical properties are strongly affected by QD size, hydrostatic pressure, as well as temperature.^[23] The absorption coefficients (AC) and refractive index (RI) spectra displayed blueshift toward higher energies with increasing pressure, but displayed redshift with increasing temperature and QD sizes. Another study performed by Yildirim et al.^[24] investigated the nonlinear part of AC of GaAs QDs and demonstrated that the AC depends on both applied electric field and geometrical asymmetry. Rezaei et al.^[25] have studied the linear and third-order nonlinear optical AC, and RI of a hydrogenic donor impurity confined in an ellipsoidal quantum dot. Using the compact-density matrix formalism and an iterative method, they found that the total RI and AC are strongly dependent on the sizes and geometry of QDs and their peaks red-shifted with increasing sizes. It has been demonstrated that the shapes of the QDs can modify the optical properties associated with band to band transition. Another study by Yesilgul et al.^[26] investigated the effects of temperature, magnetic field, and pressure on the optical responses in a symmetric double semi-V-shaped quantum well (GaAs/Al_xGa_{1-x}As), and found that the optical properties are deeply affected by temperature, magnetic field, and pressure. Kasapoglu et al.^[27] have studied the donor impurity state transitions in a 2-D QD of triangular shape under an applied electric field and found that the applied electric field may lead to quenching of interstate light absorption.

However, among the existing reports in the literature, most reports were devoted to nonlinear optical properties due to impurities; very few studied the nonlinear optical properties associated with excitonic transitions.^[23,28,29] In the case of CSQD, El Haouari et al.^[30] have determined the effect of pressure on the energy of ground state and on the optical properties of a single dopant confined in the CSQD, whose optical properties deeply depend on the shell thickness, impurity position, as well as hydrostatic pressure. AC and RI undergo a blue-shift induced by decreasing shell size or increasing hydrostatic pressure; while a red-shift is observed when impurity moves toward the edges of the shell. Zeng et al.^[31] have reported a theoretical work on the behaviors of linear, nonlinear, and total AC (TAC) and RI during the intersubband transitions of CSQDs of ZnO/ZnS and ZnS/ZnO when considering the shell thickness, impurity position, as well as dielectric effects. Ha et al. have calculated the optical properties of Al_xGa_{1-x}/AlN core/shell nanowires, and also found that they are strongly influenced by sizes, temperature, and pressure.^[32]

To our knowledge, there are yet no studies which treat the excitonic transition $1s - 1p$ in the SCSQD system. In order to further our previous study^[33] regarding the pressure effect on the energy of a confined exciton in an SCSQD (AlN/GaN), we study the effect of core/shell ratios and pressure on the linear and third-order nonlinear AC and RI during $1s-1p$ excitonic transitions of an exciton confined in this structure, to determine contribution from the excitonic state transitions to optical properties. Our calculations are carried out in the effective mass approximation (EMA) framework and the binding energies are calculated by the Ritz method, by choosing an appropriate wave function accounted for different inter-particle correlations between $1s$ and $1p$ states. This paper is structured as follows: in the section "Theoretical framework" our theoretical framework is presented to calculate the energies and the optical properties for the $1s - 1p$ intersubband transition; in the section "Results and discussion" our numerical results and discussions are provided; and in the section "Conclusions" our conclusions are given.

Theoretical framework

Determination of the energies of $1s$ and $1p$ states

To calculate the energies of $1s$ and $1p$ states, we consider a confined exciton $X(e,h)$ in a SCSQD (AlN/GaN). In the EMA framework, the Hamiltonian of the system, considering the contribution from applied pressure P , can be expressed as:

$$H_X = -\frac{\hbar^2}{2m_e^*(P)}\Delta_e - \frac{\hbar^2}{2m_h^*(P)}\Delta_h - \frac{e^2}{\varepsilon(P)r_{ch}} + V_s^e + V_s^h \quad (1)$$

In Eq. (1), $r_{ch} = |\vec{r}_e - \vec{r}_h|$, where \vec{r}_e and \vec{r}_h are the positions of an electron and hole, respectively. $m_i^*(P)$ ($i = e, h$) are the effective masses (EMs) of the electron and hole, respectively. The dielectric constant $\varepsilon(P)$, as the function of the

applied pressure, can be written as, according to Refs.^[34-36]:

$$\varepsilon(P) = 1 + (\varepsilon(0) - 1)\exp\left(-\frac{5}{3B_0}(0.9 - f_i)P\right), \quad (2)$$

where f_i is the Phillips ionicity parameter of GaN, and B_0 can be written as:

$$B_0 = \frac{(C_{11} + C_{12})C_{33} - 2(C_{13})^2}{C_{11} + C_{12} + 2C_{33} - 4C_{13}}. \quad (3)$$

The EMs of the electron and hole as the function of the applied pressure can be determined by^[37]

$$m_i^* = \frac{m_0}{1 + (C_i/E_g(P))}, \quad i = (e, h) \quad (4)$$

where m_0 is the free electron mass and C_i is a fixed value for GaN. The band gap of GaN at the center of the Brillouin zone (point Γ), $E_g(P)$, which is pressure-dependent, can be written as^[38]:

$$E_g(P) \text{ (meV)} = E_g(0) \text{ (meV)} + \vartheta P + \beta P^2. \quad (5)$$

In the above relations, the pressure is given in the unit of GPa. The band offset between AlN ($E_g = 6.2$ eV) and GaN ($E_g = 3.4$ eV) is very large, and therefore the presence probability of the carriers is important only in the GaN region (shell) and therefore the charge carriers' wave functions stay confined in the shell. As a result, an infinite potential barrier outside the shell is a good approximation to describe the problem:

$$V_s^i(r_i) = \begin{cases} 0, & \text{if } a < r_i(P) < b \\ \infty, & \text{if } r_i(P) < a \text{ and } r_i(P) > b \end{cases} \quad i = (e, h), \quad (6)$$

where a and b are the core/shell radii, respectively.

Yu et al.^[39] have demonstrated that the QD volume is strongly affected by the hydrostatic pressure effects. It can be generalized to obtain the following equation of the core/shell radii:

$$R_i(P) = R_i(0)[1 - 3P(S_{11} + 2S_{12})]^{1/3}, \quad (7)$$

$i = (\text{core, shell})$

where $R_i(0)$ is the radius when external pressure is zero. S_{11} and S_{12} are the compliance parameters of GaN defined by the elastic constants C_{11} and C_{12} in the following relations^[20,40,41]:

$$S_{11} = \frac{C_{11} + C_{12}}{(C_{11} - C_{12})(C_{11} + 2C_{12})} \quad (8)$$

and

$$S_{12} = \frac{C_{12}}{(C_{11} - C_{12})(C_{11} + 2C_{12})}. \quad (9)$$

Adopting the excitonic units $a_X = \hbar^2\varepsilon/\mu e^2$ for length and $R_X = \hbar^2/2\mu a_X^2$ for energy, where $\mu^{-1} = (m_e^*)^{-1} + (m_h^*)^{-1}$ is

the excitonic reduced mass, the Hamiltonian (1) can also be written as:

$$H_X = -\frac{1}{1 + \sigma} \left[\frac{m_e^*(0)}{m_e^*(P)} \right] \Delta_e - \frac{\sigma}{1 + \sigma} \left[\frac{m_h^*(0)}{m_h^*(P)} \right] \Delta_e - \frac{2\varepsilon(0)}{\varepsilon(P)r_{ch}}, \quad (10)$$

where $\sigma = m_e^*/m_h^*$ is the electron to hole mass ratio.

In fact, such a two-body system is well-suited to be described by the Hylleraas coordinates $(r_e, r_h, r_{ch}, z_e, z_h)$.^[42-44] So the Laplacian, for the electron (positron), can be written as:

$$\Delta_e = \frac{\partial^2}{\partial r_e^2} + \frac{2}{r_e} \frac{\partial}{\partial r_e} + \left(\frac{r_e^2 - r_h^2 + r_{ch}^2}{r_e r_{ch}} \right) \frac{\partial^2}{\partial r_e \partial r_{ch}} + \frac{2}{r_{ch}} \frac{\partial}{\partial r_{ch}} + \frac{\partial^2}{\partial r_{ch}^2} + \frac{2z_e}{r_e} \frac{\partial^2}{\partial z_e \partial r_e} + 2 \left(\frac{z_e - z_h}{r_{ch}} \right) \frac{\partial^2}{\partial z_e \partial r_{ch}} + \frac{\partial^2}{\partial z_e^2}. \quad (11)$$

For positron, Δ_h can be obtained by substituting the index e by h .

Therefore, in such a coordinate system, the Schrödinger equation is given by $H_X \Psi_X(r_e, r_h, r_{ch}, z_e, z_h) = E_X \Psi_X(r_e, r_h, r_{ch}, z_e, z_h)$. The eigenvalue energy E_X can be obtained by the minimization of the mean value of H_X :

$$E_X = \min \frac{\langle \psi_X | H_X | \psi_X \rangle}{\langle \psi_X | \psi_X \rangle} \quad (12)$$

As mentioned earlier, our study is devoted to the excitonic transition from the ground state $1s$ ($n=1, l=0, m=0$) to the first excited state $1p$ ($n=1, l=1, m=0$). For this reason, the trial wave functions can be chosen as:

$$\psi_{1s} = N_0 J_0(r_e) J_0(r_h) Y_0^0(\theta_e, \varphi_e) Y_0^0(\theta_h, \varphi_h) \exp(-\gamma r_{ch}) \quad (13)$$

$$\psi_{1p} = N_1 J_1(r_e) J_1(r_h) Y_1^0(\theta_e, \varphi_e) Y_1^0(\theta_h, \varphi_h) r_{ch} \exp(-\delta r_{ch}) \quad (14)$$

where $J_0(r_i)$ and $J_1(r_i)$ are the zero order and the first order spherical Bessel functions, respectively, considering the core and shell radii.^[23,30] N_0 and N_1 are the normalization constants. $Y_l^m(\theta, \varphi)$ represent the spherical harmonics. $\exp(-\gamma r_{ch})$ and $\exp(-\delta r_{ch})$ describe the coulombic spatial overlapping between the electron and hole for the ground and first excited states respectively. γ and δ are the nonlinear variational parameters, which must be determined in order to minimize the energy mean value E_X .

Optical properties

To discuss optical properties, we recall that the total refractive index (TRI) change is given by, based on the compact density matrix approach^[45-47]:

$$\frac{\Delta n(\omega)}{n_r} = \frac{\Delta^{(1)}n(\omega)}{n_r} + \frac{\Delta^{(3)}n(\omega, I)}{n_r} \quad (15)$$

$\Delta^{(1)}n(\omega)$ and $\Delta^{(3)}n(\omega, I)$ are the linear RI (LRI) and third-order nonlinear RI (NLRI), respectively, given by the following equations:

$$\frac{\Delta^{(1)}n(\omega)}{n_r} = \frac{1}{2\varepsilon_0 n_r^2} \frac{\sigma_1 |M_{fi}|^2 (E_{fi} - \hbar \omega)}{(E_{fi} - \hbar \omega)^2 + (\hbar \Gamma_{fi})^2} \quad (16)$$

and

$$\begin{aligned} \frac{\Delta^{(3)}n(\omega, I)}{n_r} = & -\frac{\mu_1 c I \sigma_1 |M_{fi}|^4}{\varepsilon_0 n_r^3} \frac{(E_{fi} - \hbar \omega)}{[(E_{fi} - \hbar \omega)^2 + (\hbar \Gamma_{fi})^2]^2} \\ & \times \left[1 - \frac{(M_{ff} - M_{ii})^2}{4|M_{fi}|^2 (E_{fi}^2 + (\hbar \Gamma_{fi})^2)} \right. \\ & \times \left\{ E_{fi}(E_{fi} - \hbar \omega) - (\hbar \Gamma_{fi})^2 \right. \\ & \left. \left. \times -(\hbar \Gamma_{fi})^2 \frac{2(2E_{fi} - \hbar \omega)}{(E_{fi} - \hbar \omega)} \right\} \right] \end{aligned} \quad (17)$$

In the previous expressions [(16) and (17)], $E_{fi} = E_{ff} - E_{ii}$ denotes the transition of energy between the states $1p$ and $1s$. $M_{fi} = e\psi_i | \vec{r}_e - \vec{r}_h | \psi_f = e\psi_i | r_{ch} | \psi_f$ denotes the electrical dipole moment of the transition $1s$ to $1p$ under the selection rule ($\Delta l = \pm 1$). c is the speed of light in vacuum. σ_1 is the density of electron given by: $\sigma_1 = n/V(P)$, where $V(P)$ is the volume of QD under pressure, I is the incident light intensity, μ_1 is the permeability, n_r is the RI of the GaN, ε_0 denotes the vacuum dielectric constant under zero pressure, $\hbar \omega$ is the energy of photon, Γ_{fi} is the non-diagonal matrix element, equal to $1/\tau_{fi}$, where τ_{fi} is defined as initial and final state relaxation rates. Following the same steps one can get the TAC:

$$\alpha(\omega, I) = \alpha^{(1)}(\omega) + \alpha^{(3)}(\omega, I) \quad (18)$$

The linear and third-order nonlinear parts of the AC (LAC and NLAC) are written as:

$$\alpha^{(1)}(\omega) = \omega \sqrt{\frac{\mu_1}{\varepsilon}} \frac{\sigma_1 \hbar \Gamma_{fi} |M_{fi}|^2}{(E_{fi} - \hbar \omega)^2 + (\hbar \Gamma_{fi})^2} \quad (19)$$

and

$$\begin{aligned} \alpha^{(3)}(\omega, I) = & -\omega \sqrt{\frac{\mu_1}{\varepsilon}} \left(\frac{I}{2\varepsilon_0 n_r c} \right) \frac{4\sigma_1 \hbar \Gamma_{fi} |M_{fi}|^4}{[(E_{fi} - \hbar \omega)^2 + (\hbar \Gamma_{fi})^2]^2} \\ & \left[1 - \frac{(M_{ff} - M_{ii})^2}{4|M_{fi}|^2} \left\{ \frac{3E_{fi}^2 - 4\hbar \omega E_{fi} + \hbar^2 (\omega^2 - \Gamma_{fi}^2)}{E_{fi}^2 + (\hbar \Gamma_{fi})^2} \right\} \right] \end{aligned} \quad (20)$$

Results and discussion

The purpose of this paper is to investigate how hydrostatic pressure and core/shell sizes affect optical properties, such as the

changes of the optical responses (LAC, NLAC, LRI, and NLRI) of a confined exciton in SCSQDs, the physical parameters of which are listed in Table I.

Before we start our discussion, we should note that the energy difference $E_{fi} = E_{ff} - E_{ii}$, the electric dipole moment M_{fi} , and incident electromagnetic field strength I are the main parameters affecting the optical properties, where the AC and RI expressions depend strongly on these parameters.

To show the energy difference contribution to the optical responses, and to indicate the confinement effect on these energies, shown in Fig. 1(a), the transition of the energy $E_{fi} = E_{1p} - E_{1s}$, for ($b = 2$ and $3a_x$) versus the core/shell radii ratio a/b and for different pressure values. It clearly shows that, the E_{fi} increases for small radii due to the size reduction effect. For the strong confinement, ($a = 2a_x$ for example) the energy difference includes two intervals: one between ($a/b = 0$ and $a/b = 0.6$), where it decreases and the other between ($a/b = 0.6$ and $a/b = 1$), where it increases. Whereas for larger radii (weak confinement), the energy difference is always an increasing function. We remark also that when a tends to b ($a/b = 1$), the difference $E_{1p} - E_{1s}$ is much larger because the confinement becomes very strong; therefore, the kinetic energies of the uncorrelated particles dominate, in this case, the total energy of exciton. Concerning the effects of hydrostatic pressure on E_{fi} [dashed line in Fig. 1(a)], we remark that E_{fi} increases when the pressure is applied, i.e., the pressure behaves as an additive confinement; however, the orbitals waves functions are less sensitive to pressure when $a \rightarrow b$, because of the excitonic orbital is less expansive, and therefore the correlated pair (electron-hole) is not influenced by this applied pressure.

In Fig. 1(b) we plot the variation of the electric dipole moment M_{fi} against the radii ratio a/b for $b = 2a_x$ and $3a_x$

Table I. Physical parameters of GaN material.^[34,38]

$m_c^*(0)(m_0)$	0.19	C_h (meV)	5772.2
$m_h^*(0)(m_0)$	0.37	C_{11} (GPa)	390
$\epsilon(0)$	9.5	C_{12} (GPa)	398
$E_g(0)$ (meV)	3390	C_{33} (GPa)	398
β (meV/GPa ²)	-0.32	C_{13} (GPa)	106
ϑ (meV/GPa)	39	I (MW/m ²)	600
σ	0.51	n_r	3.08
a_x (nm)	4.01	σ_1 (/m)	4.6×10^{22}
R_x (meV)	18.9	Γ_{fi} (/ps)	0.2
C_e (meV)	14,452	f_i	0.5

(solid line) and under different pressure values (dashed line). We notice that the electric dipole moment increases with decreasing SCSQD size; however on the other hand, the M_{fi} reduces when the core/shell radii ratio a/b increases and tends to 0 for $a/b \rightarrow 1$. The pressure (dashed line) has a little effect, where the M_{fi} slowly diminishes when the pressure increases. Another remark can be added: the influence of pressure is less pronounced for strong confinement ($a \rightarrow b$) than for weak confinement.

Now let us analyze how the SCSQD sizes influence the behaviors of the optical properties. We plot in Fig. 2(a) the LAC, NLAC, and TAC versus $\hbar\omega$ for two shell size values: $b = 2a_x$ and $3a_x$ and for $a = b/2$. First, we remark from Eqs. (16) and (19), that the LAC and LRI constitute the major

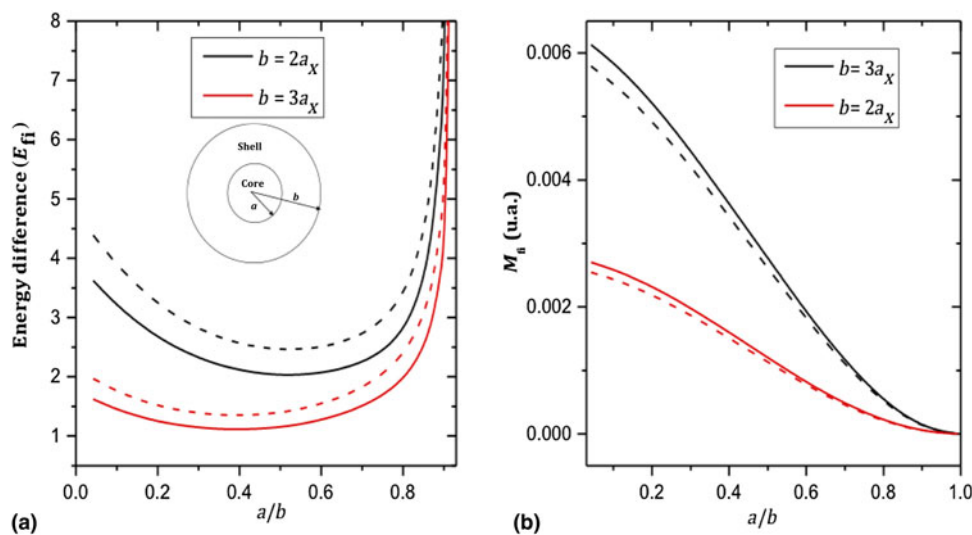


Figure 1. (a) Energy difference as a function of the radii ratio a/b : ($b = 2a_x$ and $3a_x$) and for different pressure values (solid line: $P = 0$ GPa and dashed line: $P = 4$ GPa). (b) The electric dipole moment as the function of the radii ratio a/b : ($b = 2a_x$ and $3a_x$) and for different pressure values (solid line: $P = 0$ GPa and dashed line: $P = 4$ GPa).

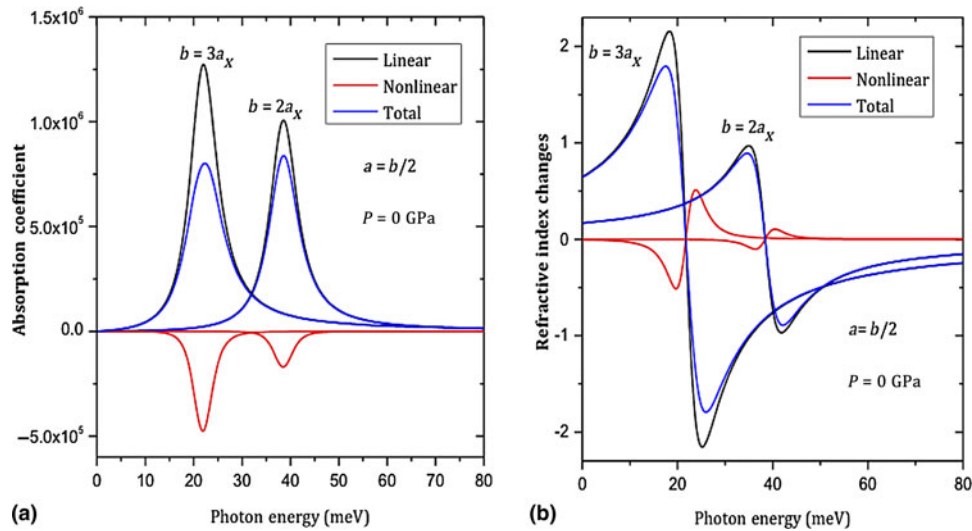


Figure 2. (a) The LAC, NLAC, and TAC versus the incident $\hbar\omega$: ($b = 2a_x$ and $3a_x$) and $a = b/2$. (b) The LRI, NLRI, and TRI versus the incident $\hbar\omega$: ($b = 2a_x$ and $3a_x$) and $a = b/2$.

contribution to the TAC and TRI, and the NAC and NRI vary oppositely with respect to the LAC and LRI terms, so the NAC and NRI terms reduce the TAC and TRI. From Fig. 2(a), we observe that the two components of the TAC have a prominent peak corresponding to the threshold frequency of the incident light. This threshold is equal to 38 and 22 meV for $b = 2a_x$ and $b = 3a_x$, respectively, so the optical AC are strongly influenced by the shell sizes where, the peaks move to the region of higher energies (blueshift) when the shell radius decreases. This behavior is related to an increase of the excitonic difference energy [Fig. 1(a)] when the radius decreases, due to the confinement effect. Indeed, the confinement effect reinforces

the coulombic particle attraction, and therefore the excitonic energies become dominating, and consequently the E_{fi} increase as the size decreases. Furthermore, we can see that the AC amplitudes decrease with the reduction of the size. This behavior can be justified by the decrease of the M_{fi} [Fig. 1(b)], when the shell radius diminishes. In Fig. 2(b), we have presented the RI against $\hbar\omega$ for $b = 2a_x$ and $3a_x$ and for $a = b/2$. As we found in the optical AC cases, the RI peaks follow the same behavior as that of the AC, they move to the low energies (redshift), and peak amplitudes increase when the confinement becomes weak.

To describe the effects of hydrostatic pressure (P) on the optical responses of a SCSQD, we plot in Fig. 3(a), the LAC,

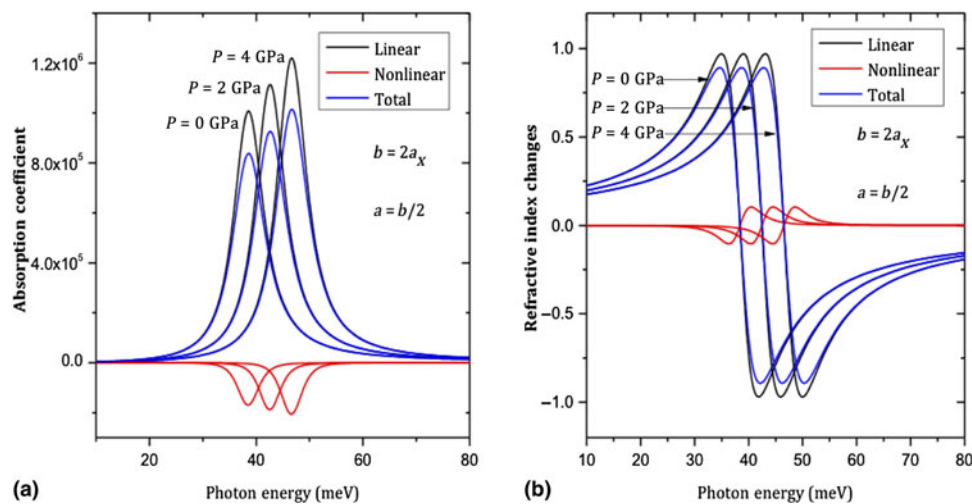


Figure 3. (a) The LAC, NLAC, and TAC versus the incident $\hbar\omega$: ($b = 2a_x$ and $a = b/2$) and for different pressure values. (b) The LRI, NLRI, and TRI versus the incident $\hbar\omega$: ($b = 2a_x$ and $a = b/2$) and for different pressure values.

NLAC, and TAC versus $\hbar\omega$ for $b=2a_x$, $a=b/2$ and under different pressure values. As expected, we see that the different curves of the optical AC are deeply affected by pressure application, and they shift to the higher energies (blueshift: shifted from 38 meV for $P=0$ to about 42.5 meV and 46.5 meV for $P=2$ and 4 GPa respectively). This is due to, on the one hand, the pressure enhances the confinement by reducing the lattice parameter of GaN material. The pressure-dependent behavior of GaN material can be generalized by the formula $a_{\text{GaN}} = a_{\text{GaN}}(1 - P/3B_0)^{[32]}$; and on the other hand, the applied pressure strongly influences the dielectric constant [Eq. (2)] and the reduced excitonic mass [Eq. (4)]. All these parameters lead to an increase of the E_{fi} [Fig. 1(a)], and consequently a shift toward high energies of the optical AC can be remarked. In Fig. 3(b), we present the variation of the LRI, NLRI, and TIR versus $\hbar\omega$ for $b=2a_x$, $a=b/2$, and for $P=0, 2$ and 4 GPa. The same behavior of the optical AC showing a blueshift with increasing pressure was found for the optical RI. Concerning the AC and RI intensities, we observe an increase and “stability” of the AC and RI peaks respectively. These behaviors can be explained based on the meaning of the AC and RI expressions. By analyzing Eqs. (19) and (20) we see that AC is related to the transition energy E_{fi} , the dielectric constant $\epsilon(P)$, and the electric dipole element M_{fi} . These parameters are functions of the pressure with different ways, which induce a competition between them. The calculus shows that the applied pressure influences $\epsilon(P)$ more than M_{fi} and E_{fi} . For the AC, the amplitudes are dominated by a pressure dependent dielectric constant, and therefore an intensity strengthening occurs. Eqs. (16) and (17) show that RI does not depend on $\epsilon(P)$, and therefore, their amplitudes are dominated by the electric dipole element which depends on P [Fig. 1(b)], which explains the “stability” of RI intensities when pressure increases.

Conclusion

Within the EMA and using variational approach, the optical properties (AC and RI) from transition between $1s$ and $1p$ states, as a function of the sizes of core/shell and pressure effect on the behavior of an exciton in a SCSQD were reported. Our results show that core/shell sizes, and applied pressure strongly affect the optical properties of the exciton. With the increasing pressure, AC and RI blueshift toward higher energies. Moreover, the electric dipole moment M_{fi} (although not affected much by pressure) increases with decreasing SCSQD size, but reduces when the core/shell radii ratio a/b tends to 0 for $a/b \rightarrow 1$. We also found that AC is strongly influenced by the shell sizes; the AC curve peaks display a blueshift when the shell radius decreases (strong confinement); the AC amplitudes also decrease with reducing shell size (strong confinement); the RI spectrum peaks follow the same behavior as AC, i.e., moves to the higher energies (redshift), and peak amplitudes decrease when the confinement becomes stronger.

References

1. F.Q. Chen, and D. Gerion: Fluorescent CdSe/ZnS Nanocrystal–Peptide Conjugates for Long-term, Nontoxic Imaging and Nuclear Targeting in Living Cells. *Nano Lett.* **4**, 1827 (2004).
2. X. Peng, and D. Battaglia: Formation of High Quality InP and InAs Nanocrystals in a Noncoordinating Solvent. *Nano Lett.* **2**, 1027 (2002).
3. S. Xu, S. Kumar, and T. Nann: Rapid Synthesis of High-Quality InP Nanocrystals. *J. Am. Chem. Soc.* **128**, 1054 (2006).
4. M. Braus, C. Burda, and M.A. El-Sayed: Variation of the Thickness and Number of Wells in the CdS/HgS/CdS Quantum Dot Quantum Well System. *J. Phys. Chem. A* **105**, 5548 (2001).
5. X. Zhong, R. Xie, Y. Basche, T. Zhang, and W. Knoll: High-Quality Violet-to Red-Emitting ZnSe/CdSe Core/Shell Nanocrystals. *Chem. Mater.* **17**, 4038 (2005).
6. W.U. Huynh, J.J. Dittmer, and A.P. Alivisatos: Hybrid nanorod-polymer solar cells. *Science* **295**, 2425 (2002).
7. R.D. Schaller, and V.I. Klimov: High Efficiency Carrier Multiplication in PbSe Nanocrystals: Implications for Solar Energy Conversion. *Phys. Rev. Lett.* **92**, 186601 (2004).
8. W.S. Coe, W.K. Woo, M.G. Bawendi, and V. Bulovic: Electroluminescence from single monolayers of nanocrystals in molecular organic devices. *Nature (London)* **420**, 800 (2002).
9. V.L. Colvin, M.C. Schlamp, and A.P. Alivisatos: Light-emitting diodes made from cadmium selenide nanocrystals and a semiconducting polymer. *Nature (London)* **370**, 354 (1994).
10. N. Tessler, V. Medvedev, M. Kazes, S. Kan, and U. Banin: Efficient near-infrared polymer nanocrystal light-emitting diodes. *Science* **295**, 1506 (2002).
11. B. Kraebel, A. Malko, J. Hollingsworth, and V.I. Klimov: Ultrafast dynamic holography in nanocrystal solids. *Appl. Phys. Lett.* **78**, 1814 (2001).
12. A.R. Kortan, R. Hull, R.L. Opila, M.G. Bawendi, M.L. Steigerwald, P.J. Carroll, and L. Brus: Nucleation and Growth of CdSe on ZnS Quantum Crystallite Seeds, and Vice Versa, in Inverse Micelle Media. *J. Am. Chem. Soc.* **112**, 1327 (1990).
13. H.S. Zhou, I. Honma, and H. Komiyama: Coated semiconductor nanoparticles; the cadmium sulfide/lead sulfide system's synthesis and properties. *J. Phys. Chem.* **97**, 895 (1993).
14. L. Spanhel, H. Weller, and A. Henglein: Photochemistry of semiconductor colloids. 22. Electron ejection from illuminated cadmium sulfide into attached titanium and zinc oxide particles. *J. Am. Chem. Soc.* **109**, 6632 (1987).
15. C.F. Hoener, K.A. Allan, A.J. Brad, A. Campion, M.A. Fox, T.E. Mallouk, S.E. Webber, and J.M. White: Demonstration of a shell-core structure in layered cadmium selenide-zinc selenide small particles by x-ray photoelectron and Auger spectroscopies. *J. Phys. Chem.* **96**, 3812 (1992).
16. J. El Khamkhami, E. Feddi, E. Assaidc, F. Dujardind, B. Stébé, and J. Diouri: Binding energy of excitons in inhomogeneous quantum dots under uniform electric field. *Physica E* **15**, 99–106 (2002).
17. J.M. Ferreyra, and C.R. Proetto: Excitons in inhomogeneous quantum dots. *Phys. Rev. B* **57**, 9061 (1998).
18. G.B. Bryant: Transport through dirty Luttinger liquids connected to reservoirs. *Phys. Rev. B* **52**, 16997 (1995).
19. I. Karabulut, and S. Baskoutas: Linear and nonlinear optical absorption coefficients and refractive index changes in spherical quantum dots: Effects of impurities, electric field, size, and optical intensity. *J. Appl. Phys.* **103**, 073512 (2008).
20. H.M. Baghramyan, M.G. Barseghyan, A.A. Kirakosyan, R.L. Restrepo, and C.A. Duque: Linear and nonlinear optical absorption coefficients in GaAs/Ga1-xAlxAs concentric double quantum rings: Effects of hydrostatic pressure and aluminum concentration. *J. Lumin.* **134**, 594–599 (2013).
21. J.C. Martinez-Orozco, K.A. Rodriguez-Magdaleno, J.R. Suarez-Lopez, C.A. Duque, and R.L. Restrepo: Absorption coefficient and relative refractive index change for a double δ -doped GaAs MIGFET-like structure: Electric and magnetic field effects. *Superlattices Microstruct.* **92**, 166–173 (2016).
22. I. Karabulut, M.E. Mora-Ramos, and C.A. Duque: Nonlinear optical rectification and optical absorption in GaAs-Ga1-xAlxAs asymmetric double

- quantum wells: Combined effects of applied electric and magnetic fields and hydrostatic pressure. *J. Lumin.* **131**, 1502–1509 (2011).
23. N. Aghoutane, M. El-Yadri, A. El Aouami, E. Feddi, F. Dujardin, M. El Haouari, C.A. Duque, C.V. Nguyen, and H.V. Phuc: Refractive index changes and optical absorption involving 1s-1p excitonic transitions in quantum dot under pressure and temperature effects. *Appl. Phys. A* **125**, 17 (2019).
 24. H. Yildirim, and M. Tomak: Optical absorption of a quantum well with an adjustable asymmetry. *Eur. Phys. J. B* **50**, 559–564 (2006).
 25. G. Rezaei, M.R.K. Vahdani, and B. Vaseghi: Nonlinear optical properties of a hydrogenic impurity in an ellipsoidal finite potential quantum dot. *Curr. Appl. Phys.* **11**, 176–181 (2011).
 26. U. Yesilgul, F. Ungan, E.B. Al, E. Kasapoglu, H. Sari, and I. Sökmen: Effects of magnetic field, hydrostatic pressure and temperature on the nonlinear optical properties in symmetric double semi-V-shaped quantum well. *Opt. Quantum Electron.* **48**, 560 (2016).
 27. E. Kasapoglu, F. Ungan, H. Sari, I. Sökmen, M.E. Mora-Ramos, and C.A. Duque: Donor impurity states and related optical responses in triangular quantum dots under applied electric field. *Superlattices Microstruct.* **73**, 171–184 (2014).
 28. E. Hanamura: Very large optical nonlinearity of semiconductor microcrystallites. *Phys. Rev. B* **37**, 1273–1279 (1988).
 29. L. Lu, W. Xie, and Z. Shu: Combined effects of hydrostatic pressure and temperature on nonlinear properties of an exciton in a spherical quantum dot under the applied electric field. *Phys. B* **406**, 3735–3740 (2011).
 30. M. El Haouari, A. Talbi, E. Feddi, H. El Ghazi, A. Oukerroum, and F. Dujardin: Linear and nonlinear optical properties of a single dopant in strained AlAs/GaAs spherical core/shell quantum dots. *Opt. Commun.* **383**, 231–237 (2017).
 31. Z. Zeng, C.S. Garoufalos, A.F. Terzis, and S. Baskoutas: Linear and nonlinear optical properties of ZnO/ZnS and ZnS/ZnO core shell quantum dots: Effects of shell thickness, impurity, and dielectric environment. *J. Appl. Phys.* **114**, 023510 (2013).
 32. S.H. Haa, H.Q. Liua, and J. Zhu: Temperature and pressure modulation on intersubband optical absorption in an Al_xGa_{1-x}N/AlN core-shell nanowire. *Superlattices Microstruct.* **123**, 183–188 (2018).
 33. N. Aghoutane, M. El-Yadri, E. Feddi, F. Dujardin, M. Sadoqi, and G. Long: Pressure effect on an exciton in a wurtzite AlN/GaN/AlN spherical core/shell quantum dot. *MRS Commun.* **8**, 527–532 (2018).
 34. S.H. Ha, and S.L. Ban: Binding energies of excitons in a strained wurtzite GaN/AlGaIn quantum well influenced by screening and hydrostatic pressure. *J. Phys.: Condens. Matter* **20**, 085218 (2008).
 35. J.-M. Wagner, and F. Bechstedt: Properties of strained wurtzite GaN and AlN: Ab initio studies. *Phys. Rev. B* **66**, 115202 (2002).
 36. C.M. Duque, A.L. Morales, M.E. Mora-Ramos, and C.A. Duque: Exciton-related optical properties in zinc-blende GaN/InGaIn quantum wells under hydrostatic pressure. *Phys. Status Solidi B* **252**, 670–677 (2015).
 37. H. Eshghi: The effect of hydrostatic pressure on material parameters and electrical transport properties in bulk GaN. *Phys. Lett. A* **373**, 1773–1776 (2009).
 38. M. Zhang, and J.J. Shi: Influence of pressure on exciton states and inter-band optical transitions in wurtzite InGaIn/GaN coupled quantum dot nanowire heterostructures with polarization and dielectric mismatch. *J. Appl. Phys.* **111**, 113516 (2012).
 39. P.Y. Yu, and M. Cordona: *Fundamentals of Semiconductors* (Springer, Berlin, 1998).
 40. F.J. Culchac, N. Porrás-Montenegro, and A. Latgé: Hydrostatic pressure effects on electron states in GaAs-(Ga, Al) As double quantum rings. *J. Appl. Phys.* **105**, 094324 (2009).
 41. M.G. Barseghyan, M.E. Mora-Ramos, and C.A. Duque: Hydrostatic pressure, impurity position and electric and magnetic field effects on the binding energy and photo-ionization cross section of a hydrogenic donor impurity in an InAs Pöschl-Teller quantum ring. *Eur. Phys. J. B* **84**, 265 (2011).
 42. F. Dujardin, E. Feddi, E. Assaid, and A. Oukerroum: Stark shift and dissociation process of an ionized donor bound exciton in spherical quantum dots. *Eur. Phys. J. B* **74**, 507 (2010).
 43. E. Feddi, A. Zouitine, A. Oukerroum, F. Dujardin, E. Assaid, and M. Zazoui: Size dependence of the polarizability and Haynes rule for an exciton bound to an ionized donor in a single spherical quantum dot. *J. Appl. Phys.* **117**, 064309 (2015).
 44. J. El Khamkhami, E. Feddi, E. Assaid, F. Dujardin, B. Stébé, and J. Diouri: Low magnetic field effect on the polarisability of excitons in spherical quantum dots. *Phys. Scr.* **64**, 504 (2001).
 45. M.R.K. Vahdani, and G. Rezaei: Influence of position-dependent effective mass on third-order nonlinear optical susceptibility of impurity doped quantum dots in the presence of Gaussian white noise. *Phys. Lett. A* **373**, 3079–3084 (2009).
 46. A.R. Jafari: Optical properties of hydrogenic impurity in an inhomogeneous infinite spherical quantum dot. *Physica B* **456**, 72–77 (2015).
 47. J. Abraham, H. Mark, and A. John Peter: Dielectric confinement on exciton binding energy and nonlinear optical properties in a strained Zn_{1-x_{in}}Mg_{x_{in}}Se/Zn_{1-x_{out}}Mg_{x_{out}}Se quantum well. *J. Semicond.* **33**, 092001 (2012).